Vol 16 No 6, June 2007
1009-1963/2007/16(06)/1719-06

Chinese Physics

© 2007 Chin. Phys. Soc.
and IOP Publishing Ltd

Polarization properties of elliptical core non-hexagonal symmetry polymer photonic crystal fibre*

Zhang Ya-Ni(张亚妮)[a)b)c)†], Miao Run-Cai(苗润才)[a)], Ren Li-Yong(任立勇)[c)],
Wang Han-Yi(王韩毅)[c)], Wang Li-Li(王丽莉)[c)], and Zhao Wei(赵卫)[c)]

[a)] *Institute of Physics and Information Technology, Shaanxi Normal University, Xi'an* 710062, *China*
[b)] *Department of Physics, Baoji College of Arts & Science, Baoji* 721007, *China*
[c)] *State Key Laboratory of Transient Optics and Photonics, Xi'an Institute of Optics and Precision Mechanics, Chinese Academy of Sciences, Xi'an* 710068, *China*

(Received 15 August 2006; revised manuscript received 9 October 2006)

In this paper, polarization properties and propagation characteristics of polymer photonic crystal fibres with elliptical core and non-hexagonal symmetry structure are investigated by using the full vectorial plane wave method. The results show that the birefringence of the fibre is induced by asymmetries of both the cladding and the core. Moreover, by adjusting the non-symmetrical ratio factor of cladding η from 0.4 to 1 in step 0.1, we find the optimized design parameters of the fibre with high birefringence and limited polarization mode dispersion, operating in a single mode regime at an appropriate wavelength range. The range of wavelength approaches the visible and near-infrared which is consistent with the communication windows of polymer optical fibres.

Keywords: birefringence, elliptical core non-hexagonal symmetry, polymer, polarization
PACC: 4281, 4281F, 4281D

1. Introduction

Photonic crystal fibres (PCFs)[1] are known to facilitate the tailoring of the modal structure of the guided light. Especially, polarization maintaining PCFs have already shown a phase birefringence as high as 1.4×10^{-3}[2] and 3.7×10^{-3},[3] comparing with the conventional design where the achievable birefringence value range from 3.1×10^{-4} for elliptical core up to 6×10^{-4} for bow-tie fibres.[4] Recently, Ortigosa-Blanch *et al*[5] presented a PCF with ultrahigh group birefringence of $G=7.5\times10^{-3}$ and approximate phase birefringence of $B=4.5\times10^{-3}$. They also observed that the phase and group birefringence in this fibre have opposite signs.

In principle, typical PCFs which preserve the six-fold symmetry have no birefringence.[6] Similar to the conventional fibres, the birefringence in PCFs can be introduced either by internal stress leading to an anisotropy of the refractive index in the core[7] (as in Panda and Bow-tie fibres), or by lowering the geometries symmetry of the fibre cross section (as in elliptical core fibres). The latter leads to strong form birefringence that less sensitive to external perturbations such as temperature, strain and pressure. Form birefringence in PCFs can be also achieved by introducing holes with different radii,[2,3,8] by replacing the circular holes with elliptical holes in the cladding,[9−11] or by adding defects to mimic an elliptical-like core.[12,13] To date, most works have concentrated on silica fibres. More recently, highly birefringent PCFs have been made in polymer[14] (also namely micro-structured polymer optical fibres, (MPOFs)). Comparing with silica PCFs, we find that polymer PCFs show a number of advantages such as the lower processing temperature of polymers, the controllability of the polymerization process, and the flexible ways to produce the polymer preforms.[15] However, no paper presents the design properties of polymer PCFs according to the light guiding characteristic of polymer. In this paper, we proposed a new design scheme on highly birefringent polymer PCFs. Several propagation characteristics of this fibre were simulated by using fully vectorial plane wave method (FV-PWM),[16,17] such as mode field properties, spectral dependence of the phase and the group birefringence, cut-off wavelengths and chromatic dispersion of phase birefringence. Moreover, by adjusting the non-symmetrical ratio factor of cladding

*Project supported by National Nature Science Foundation of China (Grant No 60437020) and the Science and Technology Plan Project of Shannxi Province (Grant No 2004K05-G47).
†Corresponding author. E-mail: zhangyn@opt.ac.cn

η from 0.4 to 1 in step 0.1, we found that the birefringence of the fibre is caused by the asymmetries of both the core and the cladding, we also found out the optimized design parameters of this fibre under high birefringence, limited polarization mode dispersion (PMD) and operating in a single mode regime approaching the visible and near-infrared regions which corresponds to the communication windows of polymer optical fibres.

2. The theory model

The cross-section of the new designed highly birefringent polymer PCFs is depicted in Fig.1.

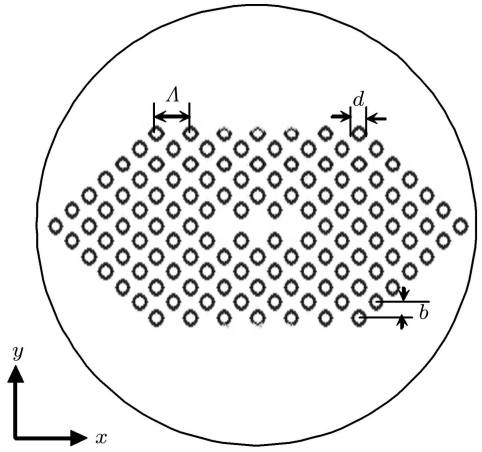


Fig.1. An elliptical core non-hexagonal symmetry structure, d is the hole-diameter, Λ is the hole-spacing in the x direction and b is the hole-spacing in the y direction.

It has a near elliptical core consisting of triple adjacent air holes defect in the core region of hexagonal structure, and the fibre cladding shows non-hexagonal symmetry structure. The geometric parameters were chosen such that the hole-spacing in x-axis direction is $\Lambda = 2.3\,\mu$m, and the ratio of hole diameter to hole-spacing in x-axis direction is $d/\Lambda = 0.4$. The non-symmetrical ratio of cladding is defined as $\eta = b/\Lambda$, which is the ratio between the hole-spacing in y-axis and that in x-axis. In the process of simulation, we neglect the material dispersion and the refractive index of background material of polymer is set as $n = 1.49$.

In order to model the propagation properties, especially the birefringence and PMD of the fibre as shown in Fig.1, the scalar approximation becomes inadequate.[18] Thus a FV-PWM has been employed to accurately predict sensitive properties. For the dielectric waveguide with linear and time-independent, lossless and free source, the equation of Helmholtz is

$$\nabla \times \frac{1}{\varepsilon(\boldsymbol{r})} \nabla \times \boldsymbol{H}(\boldsymbol{r}) = \frac{\omega^2}{c^2} H(\boldsymbol{r}), \tag{1}$$

where $\varepsilon(r)$ is dielectric constant, and $c = 1/\sqrt{\varepsilon_0 \mu_0}$ is the speed of light in vacuum.

Since the z-direction of PCFs is index-invariant, the separation of H and E field into transverse and longitudinal components is most convenient. The transverse field component obeys the following vector wave equation:

$$(\nabla_t^2 + k_0^2 \varepsilon) E_t + \nabla_t (E_t \cdot \nabla_t \ln \varepsilon) = \beta^2 E_t, \tag{2}$$

$$(\nabla_t^2 + k_0^2 \varepsilon) H_t + \nabla_t \ln \varepsilon \times (\nabla_t \times H_t) = \beta^2 H_t. \tag{3}$$

Similar to the plane wave method, we apply the periodic boundary conditions to it, assume that the dielectric constant is a periodic function of the space then it can be expanded by using Fourier series:[19]

$$\varepsilon(r) = \sum_G \varepsilon_G \mathrm{e}^{\mathrm{i}\boldsymbol{G}\cdot\boldsymbol{r}}, \quad \ln \varepsilon(r) = \sum_G k_G \mathrm{e}^{\mathrm{i}\boldsymbol{G}\cdot\boldsymbol{r}}, \tag{4}$$

where $\boldsymbol{G}$ is the grid vectors in the reciprocal space.

The transverse E field can also be expanded by using Fourier series:

$$E_t = \sum_G \left\{ E(G,x) \mathrm{e}^{\mathrm{i}\boldsymbol{G}\cdot\boldsymbol{r}} \hat{x} + E(G,y) \mathrm{e}^{\mathrm{i}\boldsymbol{G}\cdot\boldsymbol{r}} \hat{y} \right\}. \tag{5}$$

Substituting Eqs.(4) and (5) into the wave equation (2), we obtain a standard eigen-value equation:

$$-|G|^2 (E_{Gx}\hat{x} + E_{Gy}\hat{y}) + k_0^2 \sum_{G'} \varepsilon_{G-G'} (E_{G'x}\hat{x} + E_{G'y}\hat{y}) - \sum_{G'} k_{\boldsymbol{G}-\boldsymbol{G}'} [(G_x - G'_x) E_{G'x}$$
$$+ (G_y - G'_y) E_{G'y}] (G_x \hat{x} + G_y \hat{y}) = \beta^2 (E_{Gx}\hat{x} + E_{Gy}\hat{y}). \tag{6}$$

For H, we also derive a similar equation as follows:

$$-|G|^2(H_{GX}\hat{x}+H_{Gy}\hat{y})+k_0^2\sum_{G'}\varepsilon_{G-G'}(H_{G'x}\hat{x}+H_{G'y}\hat{y})-\sum_{G'}k_{\boldsymbol{G}-\boldsymbol{G'}}[(h_{G'y}G'_x-h_{G'x}G'_y)$$
$$\times[(G_y-G'_y)\hat{x}-(G_x-G'_x)\hat{y}]=\beta^2(H_{Gx}\hat{x}+H_{Gy}\hat{y}). \quad (7)$$

By solving Eqs.(6) and (7) at a particular wavelength λ, the modes and the corresponding β of the PCF can be calculated, the propagation properties of PCFs are also obtained. To ensure high accuracy to reconstruct the sub-wavelength details of the microstructure with sufficient precision, we use as many as 2^{16} plane waves per polarization and supercell comprising up to 99 elementary cells.

3. Birefringence of the cladding

To analyse the origin of anisotropic properties of elliptical core non-hexagonal symmetry cladding, we apply the concept of the fundamental space-filling mode (FSM). FSM is the fundamental mode of an infinite photonic crystal cladding when the core is absent.[1] The propagation constant β_{FSM} of the FSM is the maximum of β allowed in the cladding and the effective cladding index is defined as $n_{\mathrm{clad}}=\beta_{\mathrm{FSM}}/k$, where k is the wave vector. The FSM is usually applied to analyse the single mode conditions for PCFs and the bound mode lying below the FSM is a leaky mode. For the non-hexagonal symmetry cladding PCFs, the spectrum of the FSM can be easily found by using FV-PWM applied to a single unit cell. Finally, the effective index of the FSM can be obtained. Figure 2 shows the birefringence of FSM (defined as $B_{\mathrm{FSM}}(\lambda)=\dfrac{\lambda}{2\pi}(\beta_{\mathrm{FSM},x}-\beta_{\mathrm{FSM},y})$) as a function of wavelength for this fibre by adjusting $\eta=0.4$, 0.5, 0.6, 0.7 and 1.0. The birefringence of fundamental mode is also depicted in Fig.2 (dash line). It can be seen from Fig. 2 that discrepancy of the two polarized states is the strongest for the lowest η, and its birefringence is also highest as expected. The effective index of polarized FSM states determines the lowest effective index of the corresponding bound mode. At long wavelength, the bound mode will eventually approach the corresponding FSM. This means that the largest possible birefringence for this PCF would be the largest birefringence of the FSM. The birefringence of the FSM reduces monotonically with the reduction of wavelength except $\eta=0.4$, which is in accordance with the statement that, in short wavelengths, the vector terms in the wave equation become negligible and the accuracy of the scalar approximation improves. For $\eta=0.4$, the birefringence of FSM reaches maximum and which is higher than that of fundamental mode at wavelength $\lambda<1.75\,\mu$m. Hence, its birefringence of fundamental mode is larger than that of other values of η due to the corresponding reduction of core region with the decreasing of η. In addition, the corresponding birefringence of FSM decreases obviously with the increasing of η, and the two polarized states meet and its birefringence is almost zero when $\eta=1.0$.

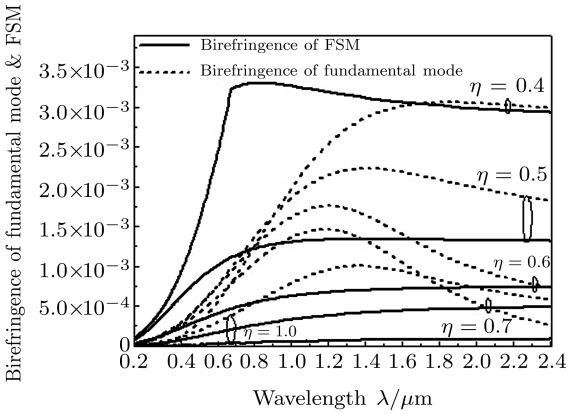


Fig.2. Birefringence of fundamental mode and FSM as a function of wavelength for $d/\Lambda=0.4$, and $\eta=0.4$, 0.5, 0.6, 0.7, 1.0.

4. Fundamental bound modes and cutoff conditions

In the case of small air-filling fraction, hexagonal symmetry lattice PCFs are well known to support only one pair of degenerate bound modes. However, in the case of large air-filling fraction, higher modes will appear because the V-parameter always has an upper bound, it can certainly exceed the cut-off of one or more higher modes.[20] Since the cut-off wavelength increases with d/Λ, in the analysis, we concentrate on the structures where d/Λ does not exceed 0.5 (here

$d/\Lambda = 0.4$). It is natural to ask how these properties are affected by the hexagonal asymmetry cladding. To show this, we introduce V-parameter for this PCF[21]

$$V_{\mathrm{PCF}}(\lambda) = \frac{2\pi a}{\lambda}\left[n_{\mathrm{c}}(\lambda)^2 - n_{\mathrm{cl}}(\lambda)^2\right]^{1/2}, \qquad (8)$$

where a is the radius of fibre core, $n_{\mathrm{c}}(\lambda)$ is the effective index of the fundamental mode associated with the index of the core, and similarly, $n_{\mathrm{cl}}(\lambda)$ is the effective index of cladding replaced by n_{FSM} here. Figure 3 shows the V-parameter as function of wavelength. It can be seen from Fig.3 that the cut-off wavelength of this fibre will increase with the decreasing of η. As η reduces from 1, the air-filling fraction of non-hexagonal symmetry cladding increases thus n_{FSM} decreases for the fixed wavelength. This leads to an increase of V. The reduction of η will also result in a reduction of core area as well as a. Hence, although the single mode region for a smaller η will less wide than that for a larger η, this region would not be reduced too much. Figure 4 shows the trajectories of the pair of fundamental modes and the pair of second-order modes as function of wavelength, here η is selected at 0.4. It should be seen that higher order modes were cut off at wavelength of 0.8μm, which accords with cut-off wavelength shown in Fig.3 when $\eta = 0.4$. Apparently, the higher modes are more dissipative due to the small core area. This extends the useful range of single-mode operation near to shorter wavelength.

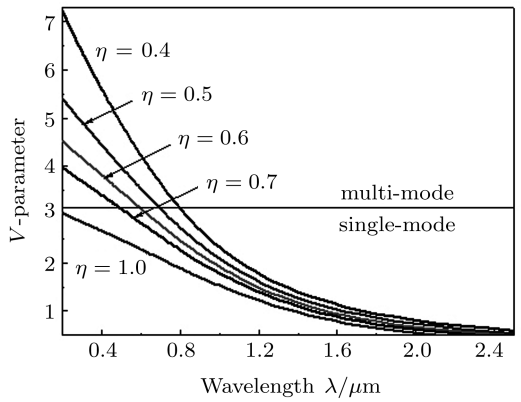


Fig.3. V-parameter as a function of wavelength for $d/\Lambda = 0.4$, and $\eta = 0.4$, 0.5, 0.6, 0.7, 1.0.

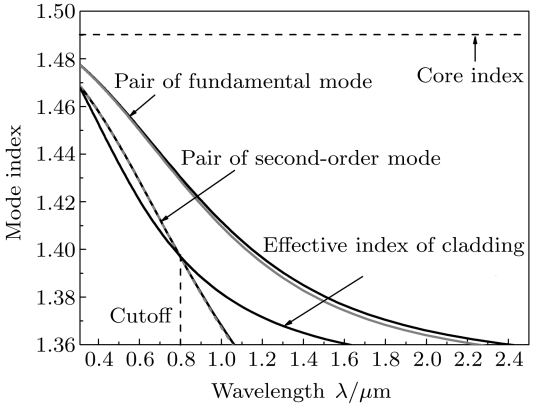


Fig.4. Modal index as a function of wavelength for $d/\Lambda = 0.4$ and $\eta = 0.4$. This fibre is multimode at wavelength $\Lambda < 0.8\,\mu$m.

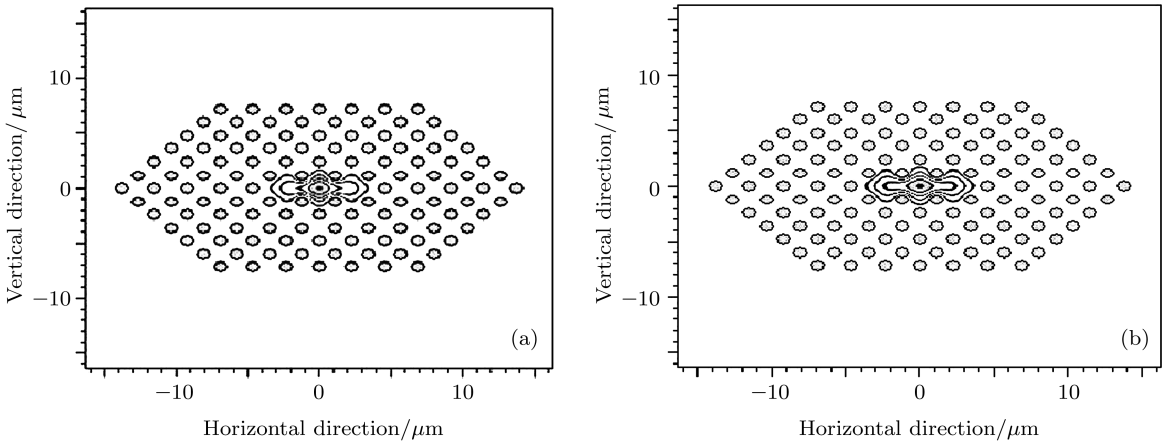


Fig.5. Intensity profiles for bound modes with $d/\Lambda = 0.4$, $\eta = 0.4$ at wavelength 850 nm (a) x component and (b) y component.

According to cutoff conditions, in order to illustrate typical modal fields, in Fig.5 we show the major components for the two fundamental modes of this fibre, with $d/\Lambda = 0.4$ and asymmetry factor $\eta = 0.4$ at wavelength $\lambda = 0.85\,\mu$m. The x-polarized mode (Fig.5(a)) with an effective index $n_{\mathrm{eff}}^{x} = 1.482824$ is more strongly bounded than that of y-polarized. The y-polarized mode (Fig.5(b)) has an effective index $n_{\mathrm{eff}}^{y} = 1.481528$, giving a birefringence $\Delta n = 0.001294$. Essentially, the bound modes are linearly

polarized along the symmetry axes. The x-mode is slightly more confined to the core and this fibre supports no other bound modes.

5. Phase and group modal birefringence

To analyse the polarization properties of the elliptical core, non-hexagonal symmetry PCF, normally two kinds of modal birefringence are defined. That is, the phase modal birefringence

$$B(\lambda) = \frac{\lambda}{2\pi}(\beta_x(\lambda) - \beta_y(\lambda)), \tag{9}$$

which is associated with the polarization beat length $L_{\mathrm{B}}(\lambda) = \lambda/B(\lambda)$, and the group modal birefringence

$$G(\lambda) = \frac{\mathrm{d}\beta_x}{\mathrm{d}k} - \frac{\mathrm{d}\beta_y}{\mathrm{d}k} = B(\lambda) - \lambda\frac{\mathrm{d}B(\lambda)}{\mathrm{d}\lambda}, \tag{10}$$

which is closely related to PMD $\tau = G/c$ and determines the rate at which orthogonal polarized pulses separate in propagation.[22] Here $\beta_{x/y}$ are the modal propagation constants and k is the free-space wave number.

Optical fibre with form birefringence (both conventional and micro-structured) typically shows significant chromatic dispersion of phase birefringence $\mathrm{d}B(\lambda)/\mathrm{d}\lambda$ and, as a result, shows a considerable difference between B and G.[23,4] Nevertheless, in many experiments with polarization maintaining fibre, these values are assumed to be equal and used interchangeably. In fact, this assumption is incorrect for the high birefringence PCFs. Figure 6 shows both the calculated phase and group birefringence for a variety of fibres with asymmetry factors $\eta = 0.4$, 0.5, 0.6, 0.7 and 1.0 over a wide range of wavelength λ spanning from $0.2\,\mu$m to $2.5\,\mu$m. It should be seen from Fig. 6 that the phase birefringence approaches zero in the shorter wavelength as expected, but in the longer wavelength, the phase birefringence will reduce and close to a non-zero constant value which does not accord with elliptical core hexagonal symmetry structured PCFs due to the existence of cladding asymmetry. As the fibre, the phase birefringence appears a maximum in an appropriate wavelength (here wavelength is between 1.0 and $1.7\,\mu$m), and the red shift of this wavelength will arise with the decreasing of η. The degeneration of the fundamental modes is significantly broken with increasing of λ for different values of η up to 1.0. The reduced splitting of two polarized modes for higher η can be clearly seen, smaller η results in higher birefringence. We assign this phenomenon to increased birefringence of FSM and the reduction of core area with the decreasing of η. The group birefringence exhibits the behaviour notably different from the phase birefringence. For short wavelength, it is negative with a minimum value at the wavelength from 0.65 to $0.95\,\mu$m, and this minimum value also induces red shift with the decrease of η. Then it rises steeply across zero, becomes significantly large and approaches to zero when wavelength becomes longer, ultimately. The appearance of zero group birefringence will depress effectively one order of PMD at wavelength regions of $0.85\mu\mathrm{m} < \lambda < 1.3\mu\mathrm{m}$, according to $\tau = G/c$. The reason for the difference between $B(\lambda)$ and $G(\lambda)$ can be found in Fig.7, showing the derivative of the phase birefringence with respect to the wavelength, which is a part of the second term in Eq.(10).

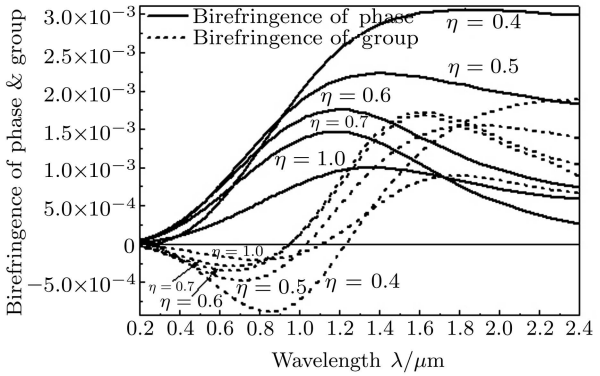


Fig.6. Birefringence of Phase and Group as a function of wavelength for $d/\Lambda = 0.4$ and $\eta = 0.4$, 0.5, 0.6, 0.7, 1.0.

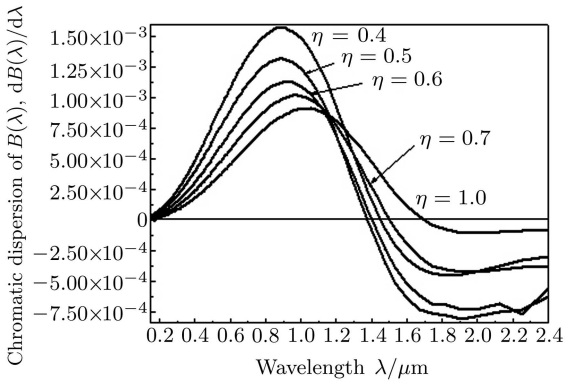


Fig.7. Chromatic dispersion of phase birefringence $\mathrm{d}B(\lambda)/\mathrm{d}\lambda$ as a function of wavelength for $d/\Lambda = 0.4$, and $\eta = 0.4$, 0.5, 0.6, 0.7 ,1.0.

The value of this term can indeed be larger than B itself. Moreover, this happens in the most interesting range of the wavelengths, namely, when $0.65\mu\mathrm{m} < \lambda < 0.95\mu\mathrm{m}$, where group birefringence is minimum. Only

in the very narrow regions (here $1.4\mu\text{m} < \lambda < 1.7\mu\text{m}$), where the derivative crosses zero, are the phase and group birefringence approximately equal. Hence, by adjusting asymmetry factor η, the designed fibre is possible to realize zero dispersion in a single mode operating within visible and near to infrared regions.

6. Conclusion

In this paper, we have shown numerically the polarization properties and propagation characteristics of elliptical core, non-hexagonal symmetry polymer PCFs by using FV-PWM. The results showed that the birefringence of the fibre is induced by asymmetries of both the cladding and the core. Moreover, by adjusting the non-symmetrical ratio factor of cladding η from 0.4 to 1 in step 0.1, we found out the optimum designing parameters of this fibre with the hole spacing of $2.3\,\mu$m in x-axis direction, $d/\Lambda = 0.4$, and non-symmetrical ratio factor of cladding $\eta = 0.4$. This fibre is able to exhibit high birefringence of 1.294×10^{-3} and limited PMD, and can operate in a single mode regime at an appropriate wavelength range. This wavelength range is approaching visible and near-infrared band which is consistent with the communication windows of polymer optical fibres. These results also provide appropriate parameters for the fabrication of highly birefringent single mode polymer PCFs. Moreover, our results indicated that it is possible to design a polarization maintaining fibre based on polymer with negligible PMD at a chosen operation wavelength, and which may be beneficial in high-bit-rate telecommunication.

References

[1] Birks T A, Knight J C and Russell P St J 1997 *Opt. Lett.* **22** 961

[2] Suzuki K, Kubota H and Kawanishi S 2001 *Opt. Express* **9** 676

[3] Ortigosa-Blanch A, Knight J C, Wadsworth W J, Arriaga J, Mangan B J, Birks T A and Russell P St J 2000 *Opt. Lett.* **25** 1325

[4] Dyott R 1995 *Elliptical Fiber Waveguides* (Norwood, MA: Artech House)

[5] Ortigosa-Blach A, Dize A, Delgado-Pinar M, Cruz J and Andres M V 2004 *IEEE Photon. Technol. Lett.* **16** 1667

[6] Steel M J and Osgood Jr R M 2001 *Opt. Lett.* **26** 229

[7] Folkenberg J R, Nielsen M D, Mortensen N A, Jacobsen C and Simonsen H R 2004 *Opt. Express* **12** 956

[8] Lou S Q, Wang Z, Ren G B and Jian S S 2004 *Chin. Phys.* **13** 1493

[9] Steel M J and Osgood R M Jr 2001 *J. of Lightwave Technol.* **19** 495

[10] Mogilevtsev D, Broeng J, Barkou S E and Bjarklev A 2001 *J. Opt. A: Pure Appl. Opt.* **3** 141

[11] Lou S Q, Wang Z, Ren G B and Jian S S 2004 *Chin. Phys.* **13** 1052

[12] Hansen T P, Broeng J, Libori E B, Knudsen E, Bjarklev A, Jensen J R, and Simonsen H 2001 *J. Photon. Technol. Lett.* **13** 588

[13] Szpulak M, Statkiewicz G, Olszewski J, Martynkien T, Urbanczyjk W, Wojcik J, Makara M, Klimek J, Nasilowski T, Berghmans F and Thienpont H 2005 *Appl. Opt.* **44** 2652

[14] Issa N A, van Eijkelenborg M A, Fellew M, Cox F, Henry G and Large M C J 2004 *Opt. Lett.* **29** 1336

[15] Zhang Y N, Li K, Wang L L, Ren L Y, Zhao W, Miao R C, Large M C J and van Eijkelenborg M A 2006 *Opt. Express* **14** 5541

[16] Ferrando A, Silvestre E, Miret J J, Andrs P and Andrs M V 1999 *Opt. Lett.* **24** 276

[17] Kotynski R, Antkowiak M J, Berghmans F, Thienpont H and Panajotov K 2005 *Opt. Quantum Electron.* **37** 253

[18] Li S G, Liu X D and Hou L T 2003 *Acta Phys. Sin.* **52** 2811 (in Chinese)

[19] Zhu Z M and Brown T G 2001 *Opt. Express* **8** 547

[20] Birks T A, Mogilevtsev D, Knight J C, Russell P St J, Broeng J, Robertst P J, Wes J A, Allan D C and Fajard J C 2000 *in Tech. Dig. Optical Fiber Communication Conf.* 1999, Washington, DC, paper FG4-1, pp 114

[21] Mortensen N A, Folkenberg J R, Nielsen M D and Hansen K P 2003 *Opt. Lett.* **28** 1879

[22] Li S G, Xing G L, Zhou G Y and Hou L T 2006 *Acta Phys. Sin.* **55** 238 (in Chinese)

[23] Legre M, Wegmuller M and Gisin N 2003 *J. Lightwave Technol.* **21** 3374